Journal of Alloys and Compounds 509 (2011) 6289–6295

Contents lists available at ScienceDirect

Journal of Alloys and Compounds

journal homepage: www.elsevier.com/locate/jallcom

Thermoelectric properties of indium-filled $In_xRh_4Sb_{12}$ skutterudites

James Eilertsen[a], Jun Li[a], Sergei Rouvimov[b], M.A. Subramanian[a,*]

[a] Department of Chemistry, Oregon State University, Corvallis, OR 97331, USA
[b] Center for Electron Microscopy & Nanofabrication, Portland State University, Portland, OR 97207, USA

ARTICLE INFO

Article history:
Received 9 February 2011
Received in revised form 5 March 2011
Accepted 9 March 2011
Available online 16 March 2011

Keywords:
Inorganic materials
Interstitial alloys
Semiconductors
Transition metal alloys and compounds
Thermoelectric materials

ABSTRACT

This study reports the synthesis and characterization of polycrystalline indium-filled $In_xRh_4Sb_{12}$ ($0 \le x \le 0.2$) skutterudites. The structural response to indium filling was monitored by whole pattern fitting of the powder X-ray diffraction data. Indium occupation of the oversized void-sites was verified by its unusually large thermal displacement parameter. The indium solubility limit approached 0.15. The principal thermoelectric properties were measured from 300 to 600 K. All samples are semiconducting. Indium void-site occupation reduced the lattice thermal conductivity of $In_{0.15}Rh_4Sb_{12}$ 30% at 300 K; however, the effect was subverted at elevated temperatures due to a coincident increase in bipolar thermal diffusion. The high-temperature thermoelectric figure of merits (*ZT*'s) are low compared to the isostructural indium-filled $In_xCo_4Sb_{12}$ skutterudites due to a striking sign change in the Seebeck coefficients at 400 K and relatively high thermal conductivities.

1. Introduction

Skutterudites are particularly promising candidates for advanced thermoelectric materials and are the focus of lasting interest due to their highly tunable transport properties. Steadfast research has produced many skutterudites with reasonably high thermoelectric figure of merits (*ZT*'s):

$$ZT = \frac{TS^2\sigma}{\kappa_L + \kappa_e} \quad (1)$$

where T is the absolute temperature, S is the Seebeck coefficient, σ is the electrical conductivity, and κ_L and κ_e correspond to the lattice and electronic components of the total thermal conductivity ($\kappa_L + \kappa_e$).

The binary skutterudite is a naturally occurring cobalt arsenide mineral containing 32 atoms per unit cell with a body-centered cubic crystal structure. A myriad of binary, ternary, and quaternary skutterudites have been synthesized from groups 8, 9, and 10 transition metal cations and from a number of chalcogen, pnictogen, and group 14 semimetal anions [1]. Substantial overlap and minor electronegativity differences between the cation and anion produces a highly covalent structure with exceptional carrier mobilities and relatively high intrinsic electrical conductivity [1,2].

In addition, skutterudites possess an open cage-like architecture with two icosahedral void-sites per unit cell. The void-site framework is comprised of antimony cages formed from a network of tilted cobalt arsenide octahedra. The void-site antimony cages can be filled with a variety of elements ranging from the alkalis, alkaline earths, and rare earths, to a number of poor metals including indium (Fig. 1a and b) [2–5]. Due to the large cage size, the filler atoms are weakly bonded, rattle (as evinced by their large thermal displacement parameters), and suppress thermal transport [1,2]. Moreover, the filler atom often contributes to the charge carrier concentration. Therefore, the *ZT* can be enhanced by both decreasing the lattice thermal conductivity and increasing the electrical conductivity [2].

Although much progress has been achieved in optimizing the *ZT* of unfilled skutterudites through transition metal and pnictogen-site doping, alloying, and nanostructuring; the most consistently effective strategy for achieving the highest ZT in skutterudites is through void-site filling. Its effectiveness is readily apparent in the indium-filled $In_xCo_4Sb_{12}$ skutterudites, where the *ZT* can be increased nearly 10 fold [3,5]. Indium suppresses the lattice thermal conductivity substantially while also donating sufficient 5p electron density to facilitate degenerate electrical conductivity [4].

As in the $In_xCo_4Sb_{12}$ skutterudites, the association between void-site substitution and lattice thermal conductivity reduction is well-known; however, the exact mechanism that causes the reduction has not been universally accepted. Guest–host quasi-harmonic coupling and filler-induced avoided crossing of phonon modes are likely explanations [6,7]. However, the theory first proposed by Slack [8], in which vibrating rattler atoms truncate phonon path lengths by resonant scattering, remains a persistent and conceptually attractive model [9].Enhanced suppression of lattice thermal conductivity has been linked to greater rattler displacement caused

* Corresponding author.
E-mail address: mas.subramanian@oregonstate.edu (M.A. Subramanian).

0925-8388/$ – see front matter © 2011 Elsevier B.V. All rights reserved.
doi:10.1016/j.jallcom.2011.03.057

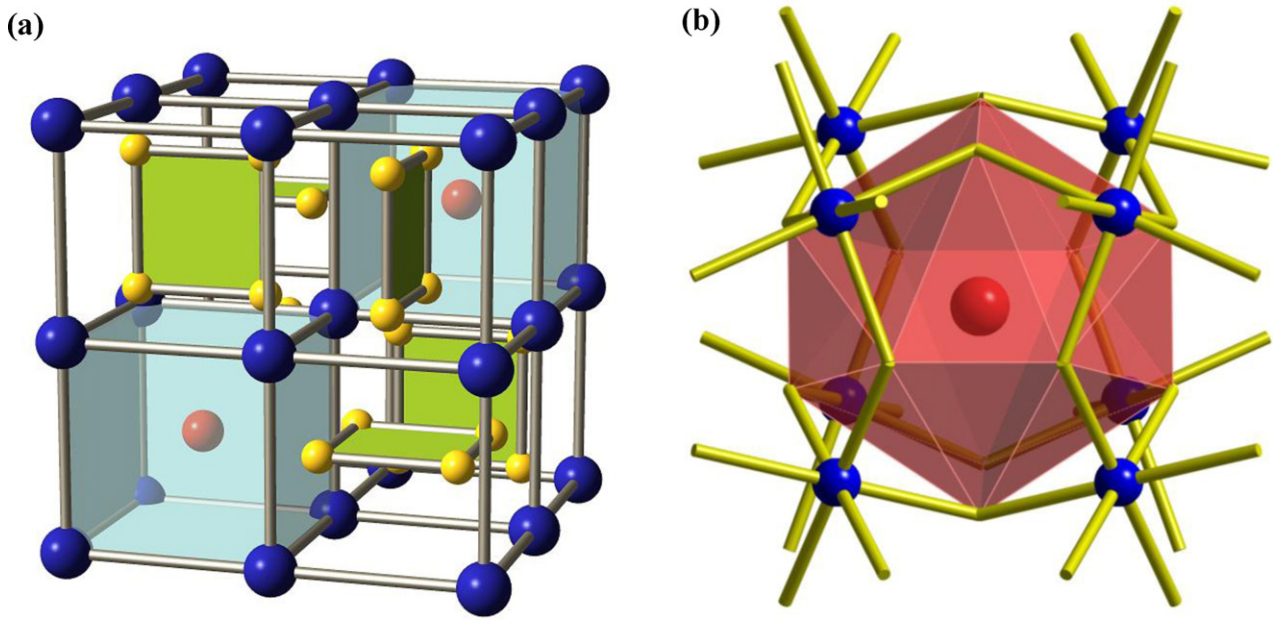

Fig. 1. The crystal structure of $In_xRh_4Sb_{12}$ showing (a) the cubic sublattice formed by Rh atoms (blue), the planar four-membered rings (green) connected by Sb_4 atoms (yellow) along the (1 0 0), (0 1 0), and (0 0 1) crystallographic directions, and the interstitial voids (turquoise cubes) with In fillers (red); (b) alternative representation of the interstitial void as an icosahedral cage (red) formed by 12 Sb atoms with In (red) "rattling" inside. The Sb atoms (end of each yellow bond) are omitted for clarity. Rh atoms (blue) are shown in the centers of tilted $RhSb_6$ octahedra. (For interpretation of the references to color in this figure legend, the reader is referred to the web version of the article.)

by filler atom radius contraction or antimony cage expansion. [10,11]. Therefore, indium-filled $In_xRh_4Sb_{12}$ may exhibit an even greater suppression compared to $In_xCo_4Sb_{12}$ due to a 7% larger void radius in the Rh_4Sb_{12} structure.

The Rh_4Sb_{12} skutterudite is a hole dominated semiconductor with strongly covalent rhodium antimony bonds. Strong covalency produces exceptional charge carrier mobility and high lattice thermal conductivity. Indium void-site occupation will likely reduce the lattice thermal conductivity, while modestly affecting carrier transport due to poor overlap. Though rhodium is an expensive element, the Rh_4Sb_{12} skutterudite is an ideal candidate for studying the interplay between void-site filling and thermal conductivity reduction.

Lanthanum, ytterbium, and iodine filled Rh_4Sb_{12} skutterudites have been reported, though these studies fail to report thermoelectric data at elevated temperatures – the temperature region where an understanding of thermal conductivity in skutterudites is most crucial [12–14]. However, this study systematically examines the effect of indium filling on all of the principal thermoelectric properties of $In_xRh_4Sb_{12}$ at elevated temperatures, with the aim of assisting current theories of thermal transport in filled skutterudites.

2. Materials and methods

Polycrystalline samples of $In_xRh_4Sb_{12}$ ($0 \le x \le 0.2$) were prepared by standard solid-state reaction. The elements In powder (99.999% Aldrich), Rh powder (99.5% Aldrich), and Sb powder (99.5% Strem) were thoroughly mixed in air in an agate mortar. The powders were loaded into alumina crucibles and reacted in a tube furnace at 610 °C for 10 h and 675 °C for 36 h under a constant flow of antimony vapor and 95%/5% N_2/H_2 gas. The furnace cooled samples were ground and loaded into a 12 mm graphite die and sintered in a uniaxial hot press at 600 °C for 60 min with a pressure of 200 MPa under a dynamic vacuum. The resultant uniaxial hot press sintered (HPS) pellets attained greater than 90% the theoretical density. For comparison, a second set of Rh_4Sb_{12} and $In_{0.1}Rh_4Sb_{12}$ samples were synthesized as above; however, these

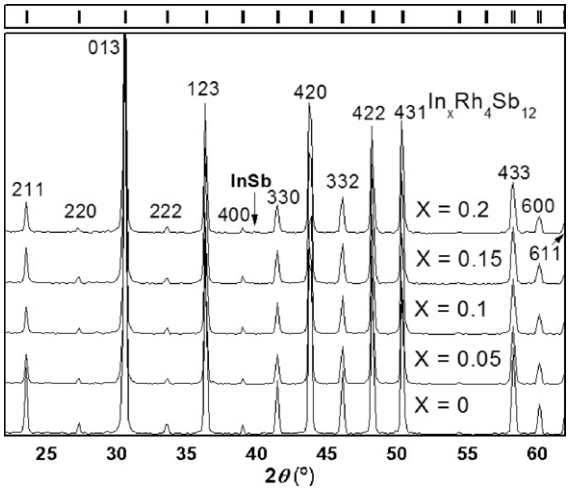

Fig. 2. XRD patterns of $In_xRh_4Sb_{12}$ ($0 \le x \le 0.2$) samples after uniaxial HPS.

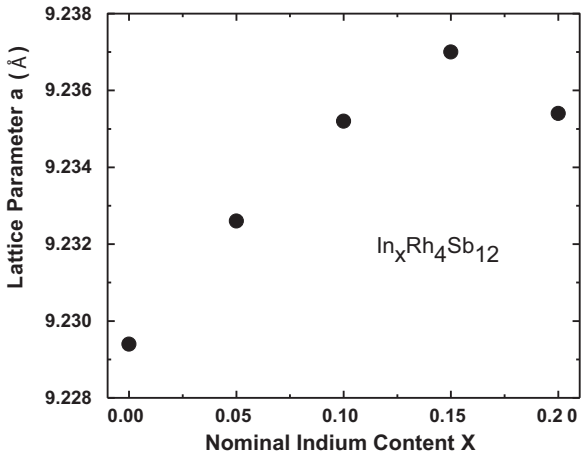

Fig. 3. Cubic cell edge a vs nominal In content x in $In_xRh_4Sb_{12}$. Error in the cubic cell edge measurements is 0.001 Å.

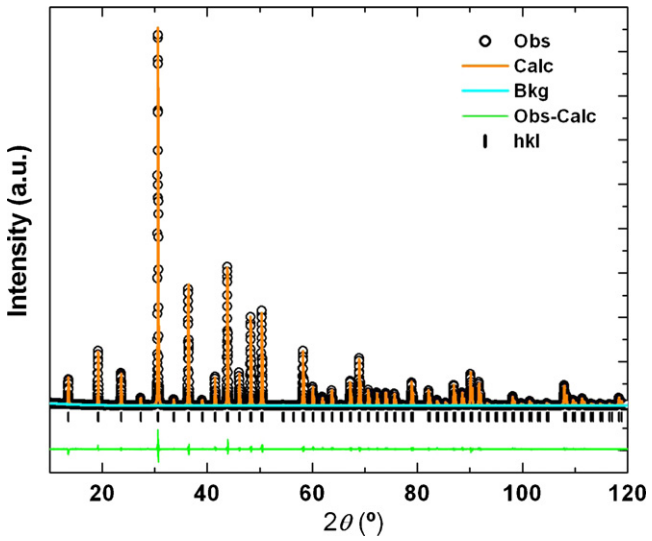

Fig. 4. Observed (open circles) and calculated (solid line) X-ray powder diffraction profiles of the $In_{0.1}Rh_4Sb_{12}$ HPS sample. The vertical bars indicate the expected reflection positions. The difference curve of $(I_{obs} - I_{calc})$ is shown at the bottom.

samples were light-pressed at room temperature into 8 mm diameter pellets and conventionally sintered at 675 °C for 6 h under a constant flow of 95%/5% N_2/H_2 gas. The resulting standard furnace sintered (SFS) pellets were approximately 60% the theoretical density.

Phase analysis of powder samples was performed by X-ray diffraction using a Rigaku MiniFlex II diffractometer with Cu Kα radiation and a graphite monochromator for the diffracted beam. Structural characterization of the $In_{0.1}Rh_4Sb_{12}$ HPS sample was carried out using data from a Rigaku D/MAX Ultima IV diffractometer with Cu Kα radiation and a graphite monochromator for the diffracted beam. A soller slit of 0.5° was used for the incident beam to reduce the axial divergence and the specimen was scanned at a step size of 0.01° and a speed of 14s per step over a 2θ range of 10–120°. Lattice parameters were calculated by LeBail fit with Si powder as an internal standard. The crystal structure of the $In_{0.1}Rh_4Sb_{12}$ HPS sample was refined by the Rietveld method using GSAS software suite [15,16]. The microstructure of the sintered samples was examined on a Quanta 600F FEG scanning electron microscope (SEM).

The principal thermoelectric properties; the Seebeck coefficient, electrical resistivity ($\rho = 1/\sigma$), and total thermal conductivity (κ_T) were measured from 300 to 600 K. The Seebeck coefficient and electrical resistivity data was collected on an ULVAC-RIKO ZEM-3 under a helium atmosphere. Thermal diffusivity (α) was measured on a Netzsch LFA 457 Micro Flash under flowing N_2 and specific heat (c_p) was measured on a Mettler Toledo 821e Differential Scanning Calorimeter with an alumina calibration standard under flowing N_2. Thermal conductivity was determined from the relation $\kappa_T = c_p \alpha d$, where d is the sample bulk density.

3. Results and discussion

3.1. Crystal structure and microstructure

Powder X-ray diffraction patterns reveal that all the $In_xRh_4Sb_{12}$ ($x \leq 0.2$) compositions crystallize in a body-centered cubic structure with space group $Im\bar{3}$. Trace InSb and antimony impurity phases were detected in all samples with indium content of $x \geq 0.1$. However, all samples with indium content of $x \leq 0.15$ became pure phase when subjected to uniaxial hot press sintering (Fig. 2). A trace amount of InSb was detected in the $x = 0.2$ sample and can be identified clearly in the diffraction pattern under magnification. Lattice variation with filling fraction indicates a solubility limit of indium close to $x = 0.15$ (Fig. 3). It is likely that the $x > 0.15$ phases are not thermodynamically stable, and are mixtures of phases with lower

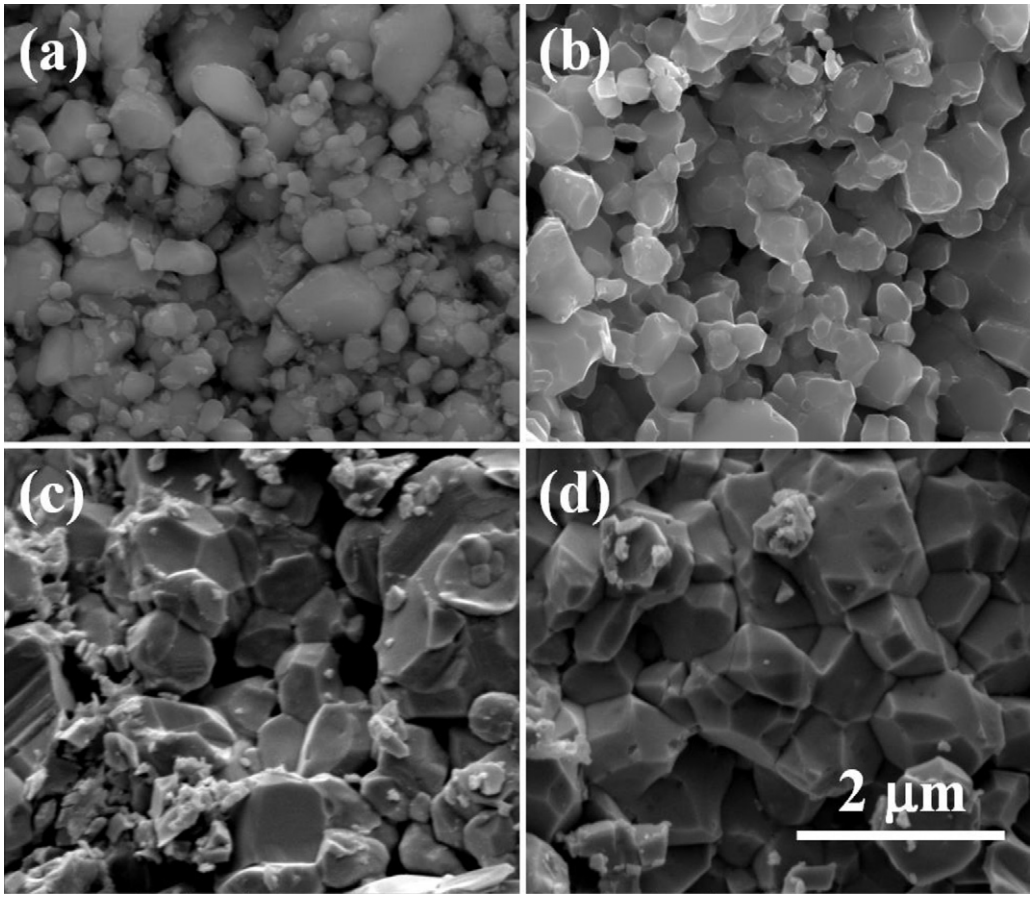

Fig. 5. Microstructure of Rh_4Sb_{12} and $In_{0.1}Rh_4Sb_{12}$ SFS (a and b) and HPS (c and d) samples. Scale bar is the same for all the images. Note the large differences in porosity between the SFS and HPS samples, and the differences in particle connectivity between the SFS samples due to the secondary InSb impurity phase.

indium content and InSb impurity; which may explain the slight downturn in lattice parameter for the nominal $x = 0.2$ sample.

The maximum indium solubility was less than the 0.22 reported for indium-filled $In_xCo_4Sb_{12}$ prepared by a similar synthesis technique [3]. Bauer et al. [13] also observed a decrease in the ytterbium solubility with an increase in transition metal size in the ytterbium-filled cobalt, rhodium, and iridium antimonide skutterudites. Lattice parameter expansion upon indium substitution was slightly smaller than the indium-filled $In_xCo_4Sb_{12}$ skutterudites due to the 7% larger void radius in the parent Rh_4Sb_{12} structure [1,3].

Rietveld refinement of the crystal structure was performed on the $In_{0.1}Rh_4Sb_{12}$ HPS sample using powder XRD data (Fig. 4). The refined crystallographic parameters are listed in Table 1. The lattice parameter (a) was determined to be 9.2375(1) Å, slightly larger than the unfilled Rh_4Sb_{12} structure. Indium occupation of the void-site was confirmed by its extremely large isotropic thermal displacement parameter (U_{iso}) as compared to Rh and Sb. In addition, Rh was found to exhibit less thermal motion around its equilibrium position as compared to Sb, which is consistent with other skutterudite systems. Attempts of refining the structure, by either including antimony or excluding indium from the void-site (2A), were not successful; nevertheless, it is probable that a small amount of indium substitutes onto the Rh site (8c). Synchrotron X-ray and neutron diffraction studies would prove useful in providing further insight into this possibility.

Table 1
Rietveld refinement of HPS $In_{0.1}Rh_4Sb_{12}$ showing large U_{iso} for the indium filler.

Atoms	Wyckoff positions	x	y	z	U_{iso} (Å^2)
Rh	8c	0.25	0.25	0.25	0.0016(7)
Sb	24g	0	0.3393(1)	0.1540(1)	0.0034(5)
In	2a	0	0	0	0.026(8)

Sb–Sb (Å)	Sb–Rh (Å), 6×	Sb–In (Å)	Rh–Rh (Å)	Sb–Rh–Sb (°)	Rh–Sb–Rh (°)
2.846(1) 2.968(1)	2.6077(2)	3.4424(5)	4.6187(2)	94.98(2)	124.65(2)

Note: The refined cell edge $a = 9.2375(1)$Å. The goodness of fit and R factors are $\chi^2 = 1.46$, wRp = 10.81% and $R_p = 7.16$%, respectively, over a 2θ range of 10–120°. The occupancy of In was refined to be 0.10(2).

Electron Dispersive Spectroscopy (EDS) analysis of the sample compositions did not indicate a large deviation from the nominal values. SEM revealed little difference when comparing the Rh_4Sb_{12} and $In_{0.1}Rh_4Sb_{12}$ HPS samples. However, further analysis of the Rh_4Sb_{12} and $In_{0.1}Rh_4Sb_{12}$ SFS samples revealed a notable difference in particle connectivity and porosity between both the filled and unfilled SFS samples between the SFS and, HPS samples (Fig. 5). The secondary InSb-impurity phase present in all of the In0.1Rh4Sb12 samples likely forms a eutectic at the primary phase surface, and during standard furnace sintering promotes greater particle con-

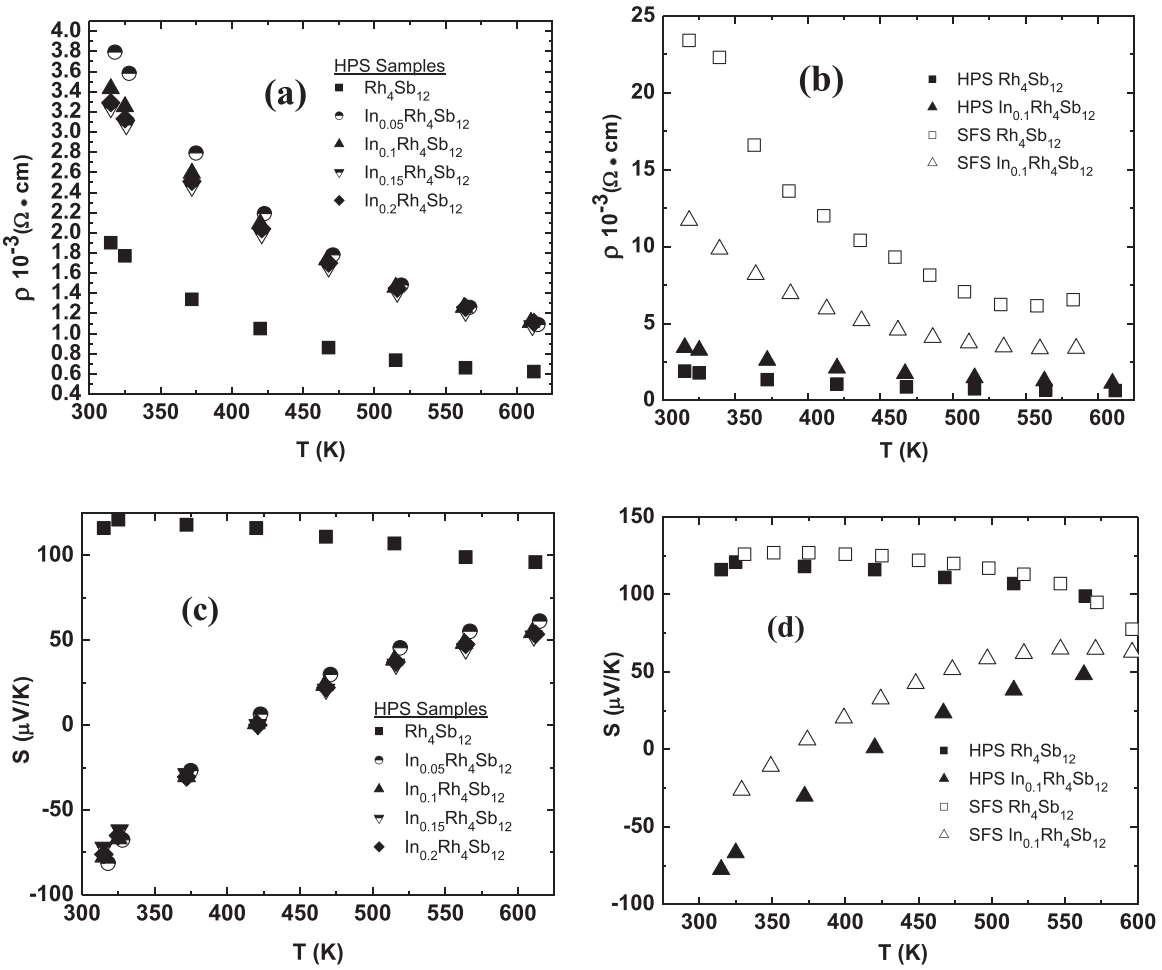

Fig. 6. Temperature dependent resistivity and Seebeck coefficient data (a and c) of $In_xRh_4Sb_{12}$ HPS samples. A comparison of $In_xRh_4Sb_{12}$ HPS (filled symbols) and SFS (open symbols) samples is shown (b and d). The SFS samples are more resistive than the HPS samples due to their higher porosity; however, little difference is observed between Seebeck coefficients.

nectivity – significantly altering electronic and thermal transport (Fig. 5a and b). However, uniaxial hot press sintering produces no microstructural variation owing to the speed and efficacy of pressure assisted sintering (Fig. 5c and d). Therefore, the observed trends in electronic and thermal transport of the HPS samples can be attributed solely to modification of the crystal structure, namely indium substitution, while trends in the transport properties of the SFS samples are distorted by differences in sample microstructure.

3.2. Electrical properties

Temperature dependent electrical resistivity data ($\rho = 1/\sigma$) of the $In_xRh_4Sb_{12}$ HPS samples, and a comparison between the SFS and HPS samples are shown (Fig. 6a and b). All samples are semiconducting, consistent with the ytterbium-filled $Yb_xRh_4Sb_{12}$ skutterudites [13]. The indium contribution to the charge carrier concentration is small compared to the degenerate indium-filled $In_xCo_4Sb_{12}$ skutterudites, due to the larger void-site radius of the Rh_4Sb_{12} system [3,5]. The indium-filled $In_xRh_4Sb_{12}$ HPS samples are slightly more resistive due to an impurity scattering mechanism activated by indium void-site substitution. Lattice expansion is expected to increase electrical conductivity in the skutterudite structure [17]. In contrast, the SFS samples exhibit the opposite trend; where the effect of the impurity scattering mechanism is concealed by the InSb modified microstructure, as discussed in Section 3.1.

The temperature dependence of the Seebeck coefficients is shown (Fig. 6c and d). The pure Rh_4Sb_{12} samples show positive (~100 μv/K) Seebeck coefficients over the entire temperature range. Conversely, the Seebeck coefficients of the indium-filled samples are negative at room temperature, they become increasingly positive at elevated temperatures, and nearly approach the value of unfilled Rh_4Sb_{12} at 600 K. The observed sign and temperature dependence of the Seebeck coefficients indicates the evident dominance of indium donated n-type carriers at low temperatures, followed by their near depletion at elevated temperatures. There is minor dissimilarity between the HPS and SFS Seebeck coefficients (Fig. 6d)

3.3. Thermal conductivity

Temperature dependent thermal conductivity data of the HPS samples and a comparison between SFS and HPS samples is shown (Fig. 7a and b). Lattice thermal conductivities were calculated from $\kappa_L = \kappa_T - \kappa_e$, and estimations of the electronic thermal conductivities were given by the Wiedemann–Franz law, $\kappa_e = L\sigma T$, where a Lorentz number (L) of $2.00 \times 10^{-8}\ V^2\ K^{-2}$, (consistent with other filled $M_xRh_4Sb_{12}$ skutterudites), was used [13,18,19]. The thermal conductivities of the SFS samples are considerably lower than the HPS samples due to the 30–38% greater porosity of the former; moreover, the order of the filled and unfilled SFS and HPS samples is revered (Fig. 7b). The indium-filled $In_{0.1}Rh_4Sb_{12}$ SFS sample possessed a thermal conductivity that was higher than the unfilled Rh_4Sb_{12} SFS sample over the entire temperature range. The reversal is due to the InSb modified microstructure as discussed in Sections 3.1 and 3.2. This finding underscores the importance of microstructural analysis when evaluating trends in thermal transport.

Indium void-site occupation reduces the thermal conductivity of the $In_{0.15}Rh_4Sb_{12}$ sample 30% at room temperature. However, while the Rh_4Sb_{12} sample showed standard inverse temperature

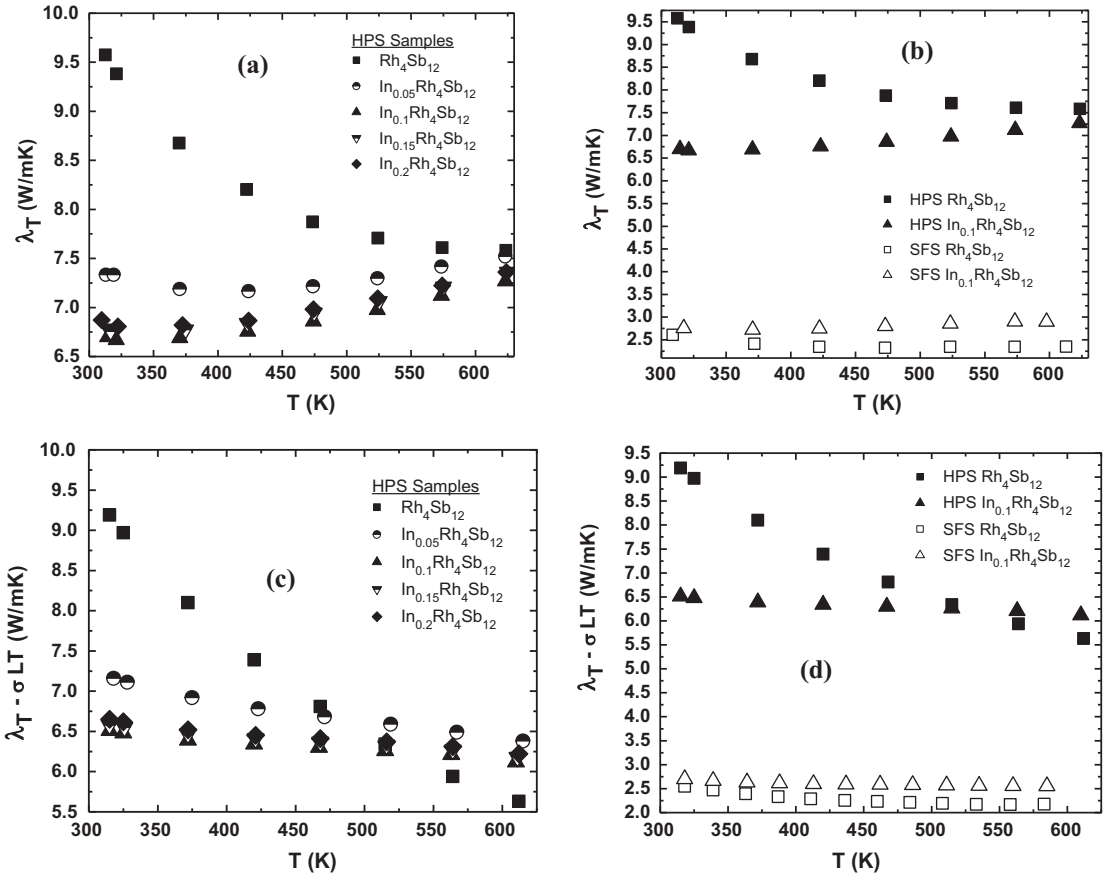

Fig. 7. Temperature dependent total and lattice thermal conductivity data (a and c) of the $In_xRh_4Sb_{12}$ HPS samples. The indium-containing samples exhibit bipolar thermal diffusion. A comparison of $In_xRh_4Sb_{12}$ HPS (filled symbols) and SFS (open symbols) samples is shown (b and c). Greater porosity in the SFS samples causes a decrease in the thermal conductivity of both filled and unfilled samples.

dependence, the thermal conductivity of the indium-filled samples increased at about 400 K. Indium void-site occupation produced virtually no reduction in thermal conductivity at elevated temperatures. The observed behavior of the indium-filled samples is attributed to a reduction in lattice thermal conductivity by the indium filler, as observed at 300 K, and a coincident increase in bipolar thermal diffusion (κ_{BP}) at higher temperatures. Bipolar thermal diffusion has been reported in intrinsic and lightly doped small band-gap semiconductors, and occurs when there is an appreciable contribution to the total electrical conductivity by both charge carriers [20,21]. It is related to the partial electrical conductivities ($\sigma_{1,2}$) and Seebeck coefficients ($S_{1,2}$) by the following:

$$\kappa_{BP} = \frac{\sigma_2 \times \sigma_2}{\sigma_2 + \sigma_2}(S_2 - S_1)^2 T \text{ and } \sigma_{1,2} = n_{1,2} e \mu_{1,2} \quad (2)$$

where $\sigma_{1,2}$ are the partial electrical conductivities; and $n_{1,2}$, e, and $\mu_{1,2}$ are the individual carrier concentration, charge, and mobility respectively. Estimation of the total electronic thermal conductivity using the Wiedemann–Franz law and static Lorenz number ignores this contribution to the total electronic thermal conductivity, which is better represented by the following:

$$\kappa_e = \kappa_{e,1} + \kappa_{e,2} + \kappa_{BP} \quad (3)$$

where $\kappa_{e,1,2}$ are the partial electronic thermal conductivities of the individual charge carriers.

Bipolar thermal diffusion is not observed in the indium-filled samples at lower temperatures (Fig. 7c). At 300 K the total electrical conductivity of the indium-filled samples is dominated by n-type charge carriers donated by indium. The sign and magnitude of the Seebeck coefficients indicate this region is far from intrinsic. Therefore, an appreciable bipolar thermal diffusion contribution is likely prohibited. However, as the indium band is progressively depleted at elevated temperatures there is a relative increase in intrinsic electrical conductivity, and a concomitant increase in bipolar thermal diffusion.

Conversely, the unfilled Rh_4Sb_{12} sample exhibited no bipolar thermal diffusion over the entire temperature range. Studies have reported a vast disparity between hole and electron mobility, 3×10^3 and 70 $cm^2V^{-1}s^{-1}$ respectively, in unfilled Co_4Sb_{12} [22]. Single-crystal studies have reported an even larger hole mobility (8×10^3 $cm^2 V^{-1} s^{-1}$) in unfilled Rh_4Sb_{12} [23]. In contrast, the hole and electron mobility ratios in intrinsic Bi_2Te_3 and Si, both known to show appreciable bipolar thermal diffusion, are one to two orders of magnitude less than the skutterudites [21,24,25]. Therefore, it is likely that a vast disparity in hole and electron mobility in completely intrinsic Rh_4Sb_{12} prohibits appreciable bipolar thermal diffusion as only one charge carrier (holes) likely dominates the electrical conductivity (Eq. (1)) [26].

These complexities do not totally prohibit evaluating the efficacy of indium filling. As contended in this section, bipolar thermal diffusion is negligible at 300 K in all samples. The observed lattice thermal conductivity reduction of the $In_{0.15}Rh_4Sb_{12}$ sample in this region is 30%. Therefore, as compared to indium-filled $In_xCo_4Sb_{12}$, indium filling is only moderately effective at reducing the lattice thermal conductivity in $In_xRh_4Sb_{12}$, contrary to what has been predicted.

The ZT of the unfilled Rh_4Sb_{12} HPS sample was higher than the indium-filled HPS samples. Indium substitution into the icosahedral void-site had a particularly deleterious effect on the Seebeck coefficients, and had little effect on the total thermal conductivities at elevated temperatures. The standard sintered samples exhibited a low ZT due to the high electrical resistivity that resulted from their high total porosity.

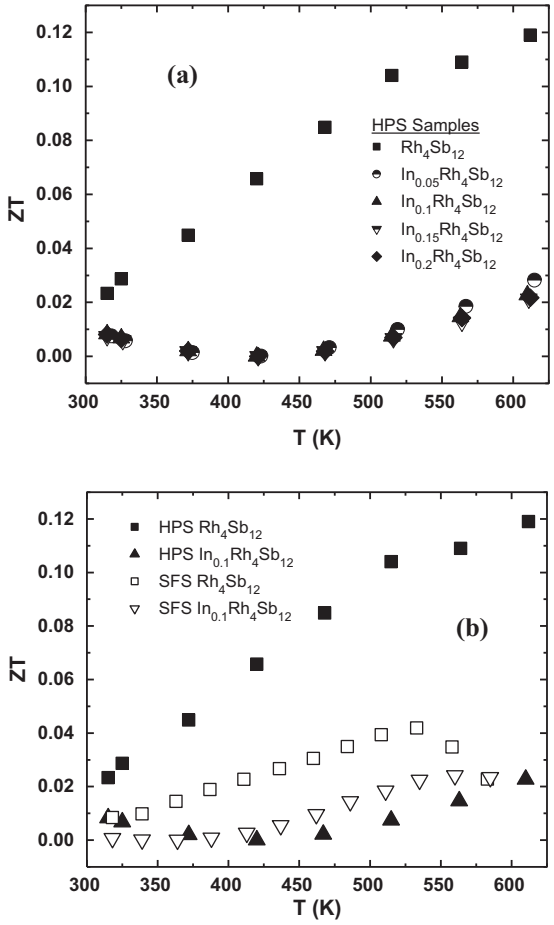

Fig. 8. Temperature dependence of ZT of (a) HPS samples $In_xRh_4Sb_{12}$ and (b) HPS (filled symbols) and SFS (open symbols) sintered samples.

4. Conclusion

Polycrystalline samples of $In_xRh_4Sb_{12}$ were synthesized with a maximum solubility limit close to 0.15. Indium insertion into the icosahedral void-site was confirmed by Rietveld analysis. The thermoelectric properties were measured from 300 to 600 K. Despite the occurrence of bipolar thermal diffusion in the indium-filled samples, it was determined that indium substitution into the icosahedral void-site only has a moderate effect on the lattice thermal conductivity. This finding is in contrast to what has been predicted for void-site-filled Rh_4Sb_{12} and may facilitate a greater understanding of the mechanism responsible for the reduction of lattice thermal conductivity in the indium-filled skutterudite systems Fig. 8.

Acknowledgements

The research completed at Oregon State University was supported by a grant from the National Science Foundation (DMR-0804167). J.E. would like to thank Dr. Jack Rundel at the Micro Products Breakthrough Institute for his assistance with the uniaxial hot press.

References

[1] G.S. Nolas, D.T. Morelli, T.M. Tritt, Annu. Rev. Mater. Sci. 29 (1999) 89–116.
[2] G.S. Nolas, J. Poon, M. Kanatzidis, in: T.M. Tritt, M.A. Subramanian (Eds.) Mater. Res. Soc. Bull. 31 (2006) 199–200.
[3] T. He, J. Chen, H.D. Rosenfeld, M.A. Subramanian, Chem. Mater. 18 (2006) 759–762.

[4] K. Akai, H. Kurisu, T. Moriyama, S. Yamamoto, M. Matsura, Proc. 17th Int. Conf. Thermoelectrics; IEEE Inc., 1998, p. 105.
[5] R.C. Mallik, J.Y. Jung, S.C. Ur, I.H. Kim, Met. Mater. Int. 14 (2008) 223–228.
[6] M.M. Koza, M.R. Johnson, R. Viennois, H. Mutka, L. Girard, D. Ravot, Nat. Mater. 7 (2008) 805–810.
[7] M. Christensen, A.B. Abrahamsen, N.B. Christensen, F. Juranyi, N.H. Andersen, K. Lefmann, J. Andreasson, C.R.H. Bahl, B.B. Iversen, Nat. Mater. 7 (2008) 811–815.
[8] J. Slack, Appl. Phys. 76 (1994) 1665–1671.
[9] D.M. Rowe, CRC Handbook of Thermoelectrics, CRC Press, Boca Raton, FL, 1995.
[10] G.S. Nolas, G.A. Slack, D.T. Morelli, T.M. Tritt, A.C. Ehrlich, J. Appl. Phys. 79 (1996) 4002–4008.
[11] M. Fornari, D.J. Singh, Appl. Phys. Lett. 74 (1999) 3666–3668.
[12] L. Zeng, H.F. Franzen, J. Alloys Compd. 311 (2000) 224–225.
[13] E. Bauer, A. Galatanu, H. Michor, G. Hilscher, P. Rogl, P. Boulet, H. Noel, Eur. Phys. J. B 14 (2000) 483–493.
[14] H. Fukuoka, S. Yamanaka, Chem. Mater. 22 (2010) 47–51.
[15] B.H. Toby, J. Appl. Crystallogr. 34 (2001) 210–213.
[16] A.C. Larson, R.B. Von Dreele, General Structure Analysis System (GSAS), Los Alamos National Laboratory, 2004, 86–784.
[17] D. Wee, B. Kozinsky, N. Marzari, M. Fornari, Phys. Rev. B: Condens. Matter Mater. Phys. 81 (2010) 045204.
[18] J.E. Parrott, A.D. Stuckes, Thermal Conductivity of Solids, Pion, London, 1975.
[19] N.W. Ashcroft, N.D. Mermin, Solid State Physics, Holt, Rinehart and Winston, New York, 1976.
[20] G.S. Nolas, H.J. Goldsmid, in: T.M. Tritt (Ed.), Thermal Conductivity: Theory, Properties, and Applications, Kluwer Academic/Plenum Publishers, New York, 2004, pp. 110–112.
[21] H.J. Goldsmid, Proc. Phys. Soc. B 69 (1955) 203–209.
[22] W.M. Haynes, D.R. Lide (Eds.), CRC Handbook of Chemistry and Physics, 2011, pp. 12–89.
[23] T. Caillat, J.P. Fleurial, A. Borshchevsky, J. Cryst. Growth 166 (1996) 722–726.
[24] I. Bejenari, V. Kantser, Phys. Rev. B: Condens. Matter Mater. Phys. 78 (2008) 115322.
[25] H.R. Shanks, P.D. Maycock, P.H. Sidles, G.C. Danielson, Phys. Rev. 130 (1963) 1743–1748.
[26] J. Yang, in: T.M. Tritt (Ed.), Thermal Conductivity: Theory, Properties, and Applications, Kluwer Academic/Plenum Publishers, New York, 2004, pp. 3–9.